J|A|C|S
A R T I C L E S

Synthesis of Periodic Hexagonal Surfactant Templated Platinum Tin Tellurides: Narrow Band Gap Inorganic/Organic Composites

Andrew E. Riley and Sarah H. Tolbert*

Contribution from the Department of Chemistry and Biochemistry, University of California, Los Angeles, Los Angeles, California 90095-1569

Received July 8, 2002; Revised Manuscript Received January 13, 2003; E-mail: tolbert@chem.ucla.edu

Abstract: In this work we report the synthesis and characterization of a new nanostructured platinum/tin/telluride inorganic/surfactant composite. The material is synthesized from soluble $SnTe_4^{4-}$ clusters and is shown to have well-defined nanometer scale periodicity along with unique optical properties. Small-angle X-ray scattering indicates that the material forms with a 2D hexagonal honeycomb structure, which is size tunable based on surfactant tail length. Multinuclear EXAFS is used as a probe of local order in these materials. The results indicate that the tetrahedral $SnTe_4$ unit dimerizes during assembly, and these clusters are coordinated to square planar platinum ions. Near-IR/visible reflectance spectroscopy indicates that the material is a narrow band gap semiconductor with a band gap of 0.8 eV. The extension of the ideas of surfactant templating to a narrow band gap semiconductor opens up the exciting potential for future optoelectronic applications.

Introduction

Self-assembly of oxide-based precursors using structure-directing agents has led to the synthesis of many novel materials with nanometer scale structure. A general class of periodic inorganic/organic composite materials has evolved from work on silica/surfactant composites.[1,2] These materials form through a cooperative self-organization process in which soluble inorganic precursors co-assemble with organic surfactants to form materials with structures reminiscent of liquid crystal phases combined with a rigid inorganic framework.[3] Removal of the organic phase from these composites results in the formation of nanoporous silicas, which have been investigated for uses varying from separation, catalysis, and host−guest chemistry to low-k dielectric coating.[4,5] These materials have many tunable properties, including pore size, wall thickness, and overall geometry of the nanometer scale periodicity. The concept of solution phase assembly of reactive inorganic precursors has also been extended beyond the silica-based materials to the formation of many different oxide-based nanostructured periodic materials such as TiO_2, ZrO_2, Nb_2O_5, SnO_2, Mn_xO_y, Al_2O_3, and others.[2,6−16] Many of these materials incorporate active catalytic

sites within their frameworks as a result of their composition, while maintaining their regular nanometer length scale periodicity.

While the proposed uses of these materials are plentiful, the development of non-oxide-based materials is an attractive pursuit because of the additional functionality of a semiconducting or metallic framework. The previous examples are generally insulators or wide band gap semiconductors because of their oxidic nature. By shifting the inorganic framework to a non-oxidic material, there is the potential to make materials that exhibit novel optoelectronic properties. Some possible uses of such materials include sensing and photocurrent applications.[17]

Solution phase assembly of non-oxide precursors presents unique synthetic challenges. Inorganic reactivity and the inability to easily use pH in nonaqueous solvents to control that reactivity limits the tools that are available for optimizing order on the nanometer length scale. Several synthetic motifs have been employed to overcome these synthetic challenges. One method is to employ stable, concentrated liquid crystalline phases that incorporate an inorganic moiety which can then be reacted to

(1) Kresge, C. T.; Leonowicz, M. E.; Roth, W. J.; Vartulli, J. C.; Beck, J. S. *Nature* **1992**, *359*, 710.
(2) Huo, Q.; Margolese, D. I.; Clesa, U.; Feng, P.; Gier, T. E.; Sieger, P.; Leon, R.; Petroff, P. M.; Schuth, F.; Stucky, G. D. *Nature* **1994**, *368*, 317.
(3) Monnier, A.; Schuth, F.; Huo, Q.; Kumar, D.; Margolese, D.; Maxwell, R. S.; Stucky, G. D.; Krishnamurty, M.; Petroff, P.; Firouzi, A.; Janicke, M.; Chmelka, B. F. *Science* **1993**, *261*, 1299.
(4) Wu, J.; Gross, A. F.; Tolbert, S. H. *J. Phys. Chem. B* **1999**, *103*, 2374.
(5) Wang, Z.; Mitra, A.; Wang, H.; Huang, L.; Yan, Y. *Adv. Mat.* **2001**, *13*, 1463.
(6) Antonelli, D. M.; Ying, J. Y. *Angew. Chem., Intl. Ed. Engl.* **1996**, *35*, 426.
(7) Bagshaw, S. A.; Pinnavaia, T. J. *Angew. Chem., Intl. Ed. Engl.* **1996**, *35*, 1102.
(8) Tian, Z. R.; Tong, W.; Wang, J.-Y.; Duan, N.-G. Krishnan, V. K.; Suib, S. L. *Science* **1997**, *276*, 926.
(9) Ciesla, U.; Schacht, S.; Stucky, G. D.; Unger, K. K.; Schuth, F. *Angew. Chem., Intl. Ed. Engl.* **1996**, *35*, 541.
(10) Yang, P.; Zhao, D.; Margolese, D. I.; Chmelka, B. F.; Stucky, G. D. *Nature* **1998**, *396*, 152.
(11) Wong, M. S.; Antonelli, D. M.; Ying, J. Y. *Nano. Mater.* **1997**, *9*, 165.
(12) Wong, M. S.; Ying, J. Y. *Chem. Mater.* **1998**, *10*, 2067.
(13) Sun, T.; Ying, J. Y. *Angew. Chem. Int. Ed.* **1998**, *37*, 664.
(14) Linden, M.; Schunk, S.; Schuth, F. In *Mesoporous Molecular Sieves*; Bonneviot, L., Beland, F., Danumah, C., Giasson, S., Kaliaguine, S., Eds.; Elsevier: Amsterdam, 1998.
(15) Soller-Illia, G. J. de A. A.; Louis, A.; Sanchez, C. *Chem. Mater.* **2002**, *14*, 750.
(16) Pidol, L.; Grosso, D.; Soller-Illia, G. J. A. A.; Crepaldi, E. L.; Sanchez, C.; Albouy, P. A.; Amenitsch, H.; Euzen, P. *J. Mater. Chem.* **2002**, *12*, 557.
(17) Rossi, M. C.; Vincenzoni, R.; Galluzzi, F. *Thin Solid Films* **1995**, *255*, 325.

form a solid inorganic framework. This approach has been used in the production of mesostructured CdS, CdSe, and ZnS.[18,19] Solution phase reduction or electrochemical deposition from liquid crystalline solutions has also been used as a route to nano-structured Pt,[20-22] Pt/Ru alloy,[23] Ni,[24] and Se,[25] although the degree of periodicity in these materials is not always very high.

By closer analogy to oxide-based materials, solution phase assembly based on the interaction between dilute surfactant solutions and ionic main group cluster ions has also been investigated. Wide band gap composite materials based on GeS,[26,27] GeSe,[27] SnS,[28] and SnSe[27,29] alloys have been synthesized using ion-exchange-based cross-linking of soluble clusters. These materials have several advantages over other nanostructured materials; specifically, the ion-exchange cross-linking route appears to yield materials with well-defined nanoscale periodicity. Additionally, these materials can be tuned not only structurally but also electronically. Changing the main group alloy or the transition metal that is used for cross-linking modulates the band gap of the final material.[27,29] Using heavier chalcogenides in the alloy appears to lead to a material with a smaller band gap. Additionally, the tin-based alloys show smaller band gaps compared to the germanium- or silica-based materials.[27-29] There is thus interest in synthesizing analogues to these systems with heavier chalcogenides to further reduce the band gap of these nanostructured materials. Smaller band gap nanostructured materials should be more efficient for use in applications that take advantage of photocurrent generation in semiconductors.[17,30-35]

To take advantage of solution phase assembly, a soluble non-oxide precursor must first be chosen. Zintl cluster chemistry provides numerous choices for small, highly charged main group clusters. Zintl clusters have been used for solution phase nanoscale assembly in both mesostructured inorganic/organic composites and nanocrystal synthesis.[26-29,36-38] Highly charged clusters are needed to drive the assembly process, which relies on strong electrostatic interactions between the polycharged clusters and polycharged surfactant micelles in solution. Additionally, there needs to be a feasible synthetic route to cross-link the inorganic cluster units.

In choosing a cluster to work with, our initial goal was to mimic the well-established chemistry of silica. To this end, the Zintl cluster K_4SnTe_4 was chosen as a monomer. This Zintl ion forms stable solutions in (degassed) water and formamide as well as several other solvents.[39,40] The $SnTe_4^{4-}$ cluster has been shown to condense via a halogen-mediated pathway to form multimers, which could be useful in cross-linking materials based on this structural subunit.[39] Upon cation exchange with high-valent transition metal ions, the cluster has also been shown to form amorphous precipitates that exhibit ion-tunable conductivity.[40] Finally, when precipitated with magnetic ions, these same alloys exhibit spin glass behavior, which could lead to magnetic coupling in the composite material based on the tin telluride cluster.[41]

In this paper we thus report the synthesis of a new platinum-bridged tin telluride material that has well-defined periodicity on the nanometer length scale. A combination of solid-state precursor synthesis and solution phase assembly is used to produce a material that is then characterized using several techniques. Small-angle X-ray scattering is used to examine the nanoscale periodicity. Platinum, tin, and tellurium EXAFS are used in correlation with elemental analysis to probe the local ordering of the inorganic framework. The thermal stability is tested using thermogravimetric analysis. Finally, the band gap of the material is measured using near-IR/visible reflectance spectroscopy.

Experimental Section

Cetyl-, octadecyl-, and eicosyl-triethylammonium bromide were all prepared by variation of an established method.[42] An excess of triethylamine was added to either 1-bromohexadecane, 1-bromoocta-decane, or 1-bromoeicosane (Acros) in ethanol. The mixture was heated in a Teflon-lined bomb at 80 °C for 3 days. The synthesis product was a liquid that upon rotary evaporation yielded a yellow-white gel. This product was then redissolved in warm chloroform (Acros) and precipitated using diethyl ether (Acros). A white powder was isolated by filtration and dried under vacuum at 100 °C.

All manipulations involving the tin telluride materials were carried out under inert atmosphere. The Zintl salt potassium tin telluride (K_4SnTe_4) was prepared via a two-step high-temperature solid-state alloying process from the constituent elements (K, Acros; Sn, Acros; Te, Acros). Equimolar potassium and tin were alloyed, followed by the exothermic alloying of equimolar amounts of KSn and tellurium. Aqueous solvent extraction, evaporation, and acetone washing yielded a dark red powder.[43] For composite assembly, 1.2 mmol of surfactant was mixed with 0.6 mmol of potassium tin telluride and then dissolved in 50.2 mmol of formamide (Acros). This mixture was agitated until completely dissolved, yielding a deep red solution. Next, 0.5 mmol of PtCl₄ (Acros) was dissolved in 25.1 mmol of formamide. This light yellow platinum(IV) solution was added to the red Zintl/surfactant mixture, resulting in the immediate precipitation of a dark solid accompanied by the liberation of heat. The whole mixture was then heated at 50 °C for 10 min. The end product was a dark powder that was isolated by filtration. When exposed to air, the material was stable for around an hour if it was still damp with formamide. It is believed that the formamide forms a protecting layer on the surface. Removal

(18) Tohver, V.; Braun, P. V.; Pralle, M. U.; Stupp, S. I. *Chem. Mater.* **1997**, *9*, 1495.
(19) Braun, P. V.; Osenar, P.; Tohver, V.; Kennedy, S. B.; Stupp, S. I. *J. Am. Chem. Soc.* **1999**, *121*, 7032.
(20) Attard, G. S.; Bartlett, P. N.; Coleman, N. R. B.; Elliott, J. M.; Owen, J. R. *Langmuir* **1998**, *14*, 7340.
(21) Attard, G. S.; Goltner, C. G.; Corker, J. M.; Henke, S.; Templer, R. H. *Angew. Chem., Intl. Ed. Engl.* **1997**, *36*, 1315.
(22) Attard, G. S.; Bartlett, P. N.; Coleman, N. R. B.; Elliott, J. M.; Owen, J. R.; Wang, J. H. *Science* **1997**, *278*, 838.
(23) Attard, G. A.; Leclerc, S. A. A.; Maniguet, S.; Russell, A. E.; Nandhakumar, I.; Bartlett, P. N. *Chem. Mater.* **2001**, *13*, 1444.
(24) Nelson, P. A.; Elliott, J. M.; Attard, G. S.; Owen, J. R. *Chem. Mater.* **2002**, *14*, 524.
(25) Nandhakumar, I.; Elliott, J. M.; Attard, G. S. *Chem. Mater.* **2001**, *13*, 3480.
(26) MacLachlan, M. J.; Coombs, N.; Ozin, G. A. *Nature* **1999**, *397*, 681.
(27) Trikalitis, P. N.; Rangan, K. K.; Kanatzidis, M. G. *J. Am. Chem. Soc.* **2002**, *124*, 2604.
(28) Rangan, K. K.; Trikalitis, P. N.; Canlas, C.; Bakas, T.; Weliky, D. P.; Kanatzidis, M. G. *Nanoletters* **2002**, *2*, 513.
(29) Trikalitis, P. N.; Rangan, K. K.; Bakas, T.; Kanatzidis, M. G. *Nature* **2001**, *410*, 671.
(30) Toyosawa, N.; Tanaka, K. *Phys. Rev. B* **1997**, *56*, 7416.
(31) Greenham, N. C.; Peng, X.; Alivisatos, A. P. *Phys. Rev. B* **1996**, *54*, 17628.
(32) Erley, G.; Gorer, S.; Penner, R. M. *App. Phys. Lett.* **1998**, *72*, 2301.
(33) Huynh, W. U.; Dittmer, J. J.; Alivisatos, A. P. *Science* **2002**, *295*, 2425.
(34) Bach, U.; Lupo, D.; Comte, P.; Moser, J. E.; Weissortel, F.; Salbeck, J.; Spreitzer, H.; Gratzel, M. *Nature* **1998**, *395*, 583.
(35) Gratzel, M. *Nature* **2001**, *414*, 338.
(36) Bley, R. A.; Kauzlarich, S. M. *J. Am. Chem. Soc.* **1996**, *118*, 12461.
(37) Taylor, B. R.; Kauzlarich, S. M. *Chem. Mater.* **1998**, *10*, 22.
(38) Yang, C.-S.; Kauzlarich, S. M.; Yang, Y. C. *Chem. Mater.* **1999**, *11*, 3666.

(39) Huffman, J. C.; Haushalter, J. P.; Umarji, A. M.; Shenoy, G. K.; Haushalter, R. C. *Inorg. Chem.* **1984**, *23*, 2312.
(40) Haushalter, R. C.; O'Connor, C. M.; Haushalter, J. P.; Umarji, A. M.; Gopal, K.; Shenoy. *Angew. Chem., Int. Ed. Engl.* **1984**, *23*, 169.
(41) Haushalter, R. C.; O'Connor, C. J.; Umarji, A. M.; Shenoy, G. K.; Saw, C. K. *Solid State Comm.* **1984**, *49*, 929.
(42) Menger, F. H.; Littau, C. A. *J. Am. Chem. Soc.* **1993**, *115*, 100083.
(43) Teller, R. G.; Krause, L. J.; Haushalter, R. C. *Inorg. Chem.* **1983**, *22*, 1809.

of the formamide using solvent exchange and vacuum leads to a dry material that rapidly oxidizes (<10 s) in air.

X-ray diffraction was carried out using a Rigaku Ultra X 18 generator producing Mo Kα radiation. A Roper Scientific 1242 × 1156 cooled X-ray CCD detector was used to record both small-angle and high-angle diffraction data. The data were collected using a $\theta-2\theta$ geometry. Samples were held in a steel cell with Mylar windows to maintain an inert atmosphere during the diffraction experiments.

Extended X-ray absorption fine structure (EXAFS) experiments were carried out on end stations 10-2, 9-3, and 4-1 at the Stanford Synchrotron Radiation Laboratory (SSRL). Data were collected at temperatures below 100 K using either a liquid nitrogen or liquid helium cryostat. Samples were loaded into an aluminum cell with Mylar windows to maintain an inert atmosphere. All data were collected in transmission geometry. Absorbance measurements were carried out at the platinum L_3 edge (11 564 eV), the tin K edge (29 200 eV), and the tellurium K edge (31 814 eV). Data analysis was performed using the EXAFSPAK software.[44] FEFF7 was used to generate phase and amplitude contributions for single and multiple scattering pathways.[45] Due to the lack of crystallographic data, several models for FEFF calculations were constructed on the basis of analogous crystallographic data using low-level force fields and energy minimizations.

A series of standard compounds were also used to determine the position of the edge jump as a function of oxidation state. For the platinum L_3 edge, platinum foil, platinum(II) chloride (Acros), and platinum(IV) chloride (Acros) were used. Tin and tellurium edge information was determined using tin foil, tellurium powder, and K_4SnTe_4. The position of the edge was assigned to the inflection point of the edge jump, as determined from the second derivative of the X-ray absorption data.

Elemental analysis was performed by Desert Analytics (P.O. Box 41838, Tucson AZ 85717). The sample was analyzed for platinum, tin, tellurium, carbon, nitrogen, hydrogen, and chlorine. Thermogravimetric analysis was performed using a Perkin-Elmer Pyris I TGA. The sample was heated at 10 °C/min from 50 °C to 600 °C in an atmosphere of flowing nitrogen. For this experiment, the sample was loaded into a TGA pan in an inert environment and quickly transferred to the instrument to avoid lengthy exposure to air.

Near−IR/UV−visible reflectance was collected using a Shimadzu UV-3100 spectophotometer. Because of the optical density of the samples, reflectance data were taken utilizing an ISR-3100 integrating sphere attachment. The collection was made over the wavelength range 2400−200 nm. The samples were pressed as a coating on a barium sulfate pellet sealed with a glass cover to maintain an inert atmosphere and a second barium sulfate pellet was used as an internal reference.

Transmission electron microscopy was taken at the CEMMA at the University of Southern California using a Philips EM420 electron microscope. Samples were prepared by depositing composite on copper grids from a drop of formamide. The excess formamide was wicked away using a clean kimwipe, and the grids were placed under vacuum for 2 h. All manipulations were carried out under inert atmosphere with the exception of loading the grid into the TEM, where the grids were briefly exposed to air.

Results

A. Composite Assembly and Characterization of Nanoscale Architecture. The synthesis of platinum tin telluride composites utilizes electrostatically driven solution phase assembly. The mixture of tin telluride clusters and surfactant is stable for moderate periods of time (>1 h) in a formamide solution. Addition of the platinum chloride results in cluster agglomeration into larger species. These larger cluster species
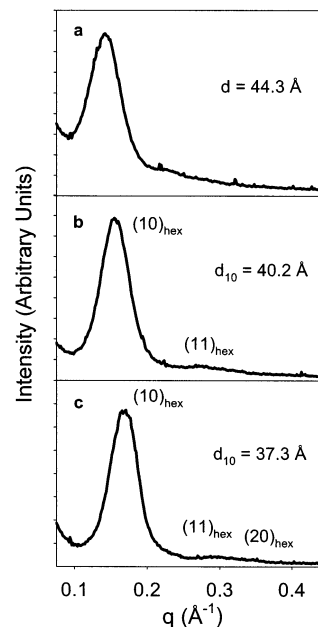
(44) http://www-ssrl.slac.stanford.edu/exafspak.html.
(45) Ankudinov, A. L.; Ravel, B.; Rehr, J. J.; Conradson, S. D. *Phys. Rev. B* **1998**, *58*, 7565. http://leonardo.phys.washington.edu/feff/.

Figure 1. Low-angle X-ray scattering from platinum tin telluride composite materials synthesized using surfactants with different tail lengths: (a) C_{20}-TEAB, a surfactant with a 20-carbon tail produces composites that show a fundamental diffraction peak with no overtones; (b and c) C_{18}TEAB and C_{16}TEAB surfactants (respectively) show the (10) and (11) peaks of a two-dimensional hexagonal phase. In part (c), the (20) peak of this phase can also be indexed. Note that the fundamental diffraction peak moves to smaller q, or larger d spacing, as the surfactant tail length increases.

can associate with the surfactant micelles without as large of an entropic penalty as that required for single cluster/micelle association.[46] The result is precipitation of the nanostructured material.

Figure 1 shows small-angle X-ray scattering for a series of as-synthesized platinum tin telluride composite materials heated at 50 °C for 10 min. The (10) and (11) diffraction peaks at distances of 1:√3 indicate a *p6mm* two-dimensional hexagonal morphology with fundamental repeat distances of 37.3 and 40.2 Å for C_{16}TEAB and C_{18}TEAB, respectively. A (20) diffraction peak can also be seen for materials synthesized with C_{16}TEAB. C_{20}TEAB shows only a fundamental diffraction peak at 44.3 Å. The poorer order in the dodecyltriethylammonium surfactant is probably related to thermal disorder of the alkyl tail in the organic. No sharp high-angle diffraction peaks are observed for any of these materials, indicating that they are amorphous on the atomic scale. If the materials are allowed to oxidize in air, the low-angle diffraction loses its peaks, indicating loss of nanoscale order.

Varying the length of the alkyl tail on the surfactant predictably affects the composite structure. The position of the fundamental diffraction peak $(10)_{hex}$ moves to larger d spacings for longer surfactant tails. This trend is in keeping with previous results from both oxide and non-oxidic species.[2,27,47] The slope of a linear fit to the data is 1.8 Å/carbon compared to a slope of 2.1 Å/carbon for GeSe systems and ∼2.3 Å/carbon in analogous silica systems.[2,47] This suggests that the alkyl chains of

(46) Monnier, A.; Schuth, F.; Huo, Q.; Kumar, D.; Margolese, D.; Maxwell, R. S.; Stucky, G. D.; Krishnamurty, M.; Petroff, P.; Firouzi, A.; Janicke, M. B.; Chmelka, F. *Science* **1993**, *261*, 1299.
(47) Watchhold, M.; Rangan, K. K.; Lei, M.; Thorpe, M. F.; Billinge, S. J. L.; Petkov, V.; Heising, J.; Kanatzidis, M. G. *J. Solid State Chem.* **2000**, *152*, 21.
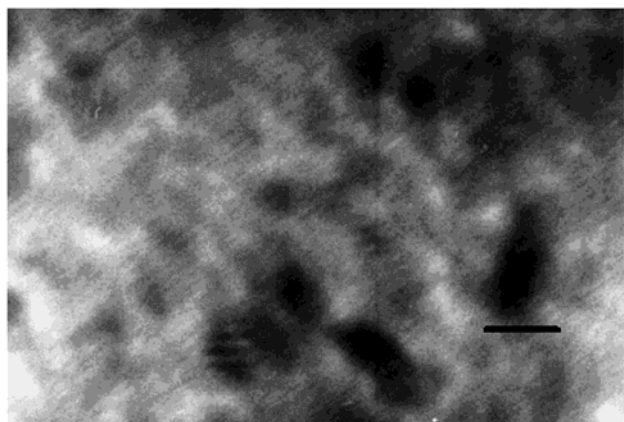
Figure 2. Transmission electron micrograph of a nanostructured platinum tin telluride composite material (scale bar is 10 nm). The picture shows lattice fringes associated with viewing a 2D hexagonal phase normal to the *c*-axis. The striations of the fringe pattern have a repeat distance that is a fraction of the center-to-center distance observed in low-angle X-ray diffraction. Viewing down the 10_{hex} axis gives a repeat distance comparable to the fundamental X-ray repeat distance (~4 nm). This is seen in some grains in the TEM, which are at a different orientation from the background striations. The background striations have a repeat distance of ~2 nm, which is expected for viewing the composite down the 11_{hex} axis.

the surfactant are somewhat more disordered in these materials compared to composites synthesized from lighter elements.

Transmission electron microscopy is used as a second method to characterize the nanoscale architecture of the material. Figure 2 shows a TEM picture of lattice fringes in the composite material. The image shows striations consistent with lattice fringes of a 2D hexagonal morphology. The stripes correspond to looking at the material perpendicular to the hexagonal *c*-axis. The apparent spacing between most of the stripes is ~2 nm, which is a spacing that corresponds to viewing down the 11_{hex} axis. In the TEM image, there are also several grains which are distinguished by having different orientations and a larger periodic spacing. These grains have a repeat distance of ~4 nm and correspond to viewing the material down the 10_{hex} direction. The observed TEM repeat distances correlate well with the low-angle X-ray diffraction and confirm the hexagonal morphology of the material.

The elemental ratios in the material (%C 25.3; %H 6.1; %N 15.1; %Te 30.8; %Pt 4.6; %Sn 10.5) indicate that the overall composition of a composite synthesized using cetyltriethylammonium bromide is $CTEA_{2.2}Pt_{1.1}(Sn_{2.0}Te_{5.5})_2$ with 38% of the overall mass being residual solvent (a mixture of the highly nonvolatile formamide and ethylenediamine, a glovebox contaminant). The amount of surfactant and residual solvent was determined using a system of three equations involving the known carbon, hydrogen, and nitrogen content of the formamide, ethylenediamine, and cetyltriethylammonium bromide and the measured mass fractions of each element. As an independent check of these calculations, if the unaccounted for mass is assumed to be oxygen, the mole fraction of formamide can be calculated because formamide is the only oxygen-containing molecule in the composite. Near perfect agreement is found between the two calculations. Incorporation of ethylenediamine in the material was predicted, as it is a contaminant in the glovebox where sample preparation took place. Additionally, the material contains no significant amounts of potassium, bromine, or chlorine, the counterions to the synthesis salts (all less than 0.1 mass %).

Most noticeable in the elemental analysis is the fact that the tin-to-tellurium ratio varies from that found in the starting material, $SnTe_4^{4-}$. The lower tin-to-tellurium ratio of 2.73 suggests the formation of new tin telluride clusters. While the ratio does not match any one tin telluride oligomer exactly, it suggests the material has a majority if its tin telluride is either $Sn_2Te_6^{4-}$ or $Sn_4Te_{10}^{4-}$.[40,48,49] The $Sn_2Te_6^{4-}$ cluster can be formed by a relatively straightforward dimerization of the starting cluster, so this species should be the kinetically favored building block. The condensation of $SnTe_4^{4-}$ clusters into large species is generally thought to be controlled by either cation-mediated ion pairing or halogen-catalyzed tellurium elimination.[48,50] Both of these routes would be available in the platinum tin telluride system.

Assuming a formal charge of +4 for each tin atom, −2 for each tellurium atom, +4 for each Pt atom, and +1 for each surfactant molecule, the composite should have a net charge of +0.6 per formula unit based on the elemental analysis results. Since elemental analysis indicates that no additional ions are present in the composite to compensate this charge, it is likely that there is redox chemistry taking place in solution that modifies some of these oxidation states prior to assembly of the final charge neutral material. Solution phase reduction of one of the positively charged ions is the most plausible way to achieve charge neutrality, and the most probable candidate for reduction is the platinum(IV) ion, which EXAFS shows to be redox active (see below). To produce a neutral composite, the average oxidation state of the platinum would have to be reduced from +4 to +3.45. Redox chemistry probably leads to a combination of platinum(IV) and platinum(II) in solution, with a likely reductant being Te^{2-} ions liberated during the dimerization of the tin telluride clusters. To achieve overall charge neutrality in the final composite, 73% of the platinum that forms the composite would need to be in a +4 oxidation state and 27% would need to be reduced down to a +2 oxidation state.

B. EXAFS Analysis and Characterization of Atomic Scale Bonding. Platinum Reduction from the Edge Jump. The position of the X-ray absorption edge jump for a given element is dependent on its oxidation state, and thus the absorption edge can be used to examine the oxidation state of Pt in these composites.[51] By calibrating against a standard (usually the pure element), ΔE_o, the shift in position of the absorption edge can be measured. Figure 4 shows the shift of E_o versus oxidation state of platinum. The as-synthesized platinum tin telluride composites show a ΔE_o of 1.3 eV, which corresponds to an intervalence state close to Pt^{2+}. Since elemental analysis indicates that the majority (73%) of the Pt comes to the composite in the 4+ oxidation state, this result leads us to the conclusion that redox chemistry must occur during composite assembly between platinum and the tin telluride species, both of which remain in the composite. On the basis of electrochemical potentials, the most likely species for oxidation is the Te^{2-}, and so composites probably contain some Te^{1-} which is bonded to the Pt^{2+}.

The presence of almost exclusively Pt^{2+} in the composite indicates that redox chemistry between platinum and the tin

(48) Ansari, M. A.; Bollinger, J. C.; Ibers, J. A. *Inorg. Chem.* **1993**, *32*, 231.
(49) Pirani, A. M.; Mercier, H. R. A.; Dixon, D. A.; Borrmann, H.; Schrobilgen, G. J. *Inorg. Chem.* **2001**, *40*, 4823.
(50) Campbell, J.; Devereux, L. A.; Gerken, M.; Mercier, H. P. A.; Pirani, A. M.; Schrobligen, G. J. *Inorg. Chem.* **1996**, *35*, 2945.
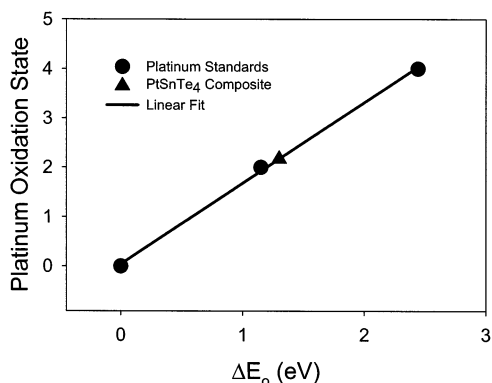(51) Teo, B. K. *EXAFS: Basic Principles and Data Analysis*; Springer-Verlag: Berlin, 1986.

Figure 3. Edge shift of the platinum L_3 edge EXAFS versus the oxidation state of platinum. Data from the hexagonal platinum tin telluride composites discussed in this work show an energy shift that is indicative of a platinum-(II) species.
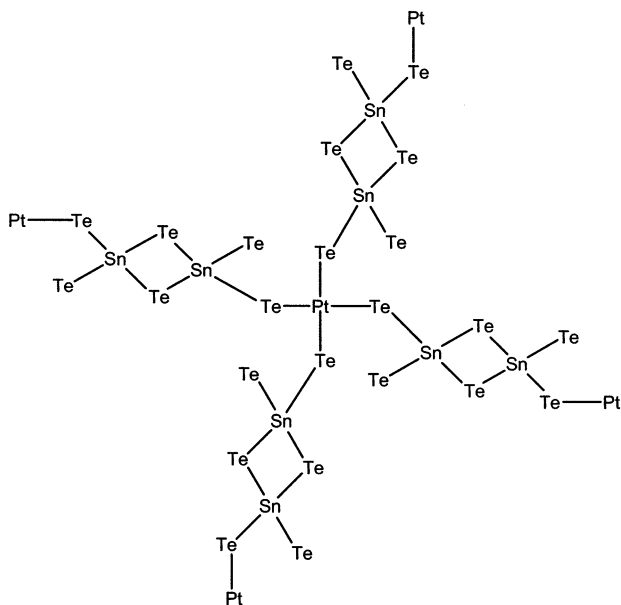
Table 1. Summary of Model Fit for Tellurium EXAFS[a]

	N	R (Å)	σ^2 (10^{-5} Å^2)	ΔE_o
Pt	0.33	2.66	78	6.328
Sn	0.33	2.67	78	6.328
Sn	0.33	2.77	78	6.328
Sn	0.33	2.78	78	6.328
Sn	0.33	2.79	78	6.328
Te	0.67	3.76	81	6.328
Te*	0.33	4.53	127	6.328
Te	0.33	5.32	156	6.328

[a] Values are obtained by fitting the EXAFS data to the model shown in Figure 3. The one exception is the Te–Te distance indicated with an asterisk. The full model predicts larger amplitude in the region around 4.5 Å, which is not found in the data because of disorder in the tin telluride tetrahedra. For purposes of fitting, all related Te–Te intracluster paths are replaced by a single path to reduce the intensity of this peak and simulate the disordered system.
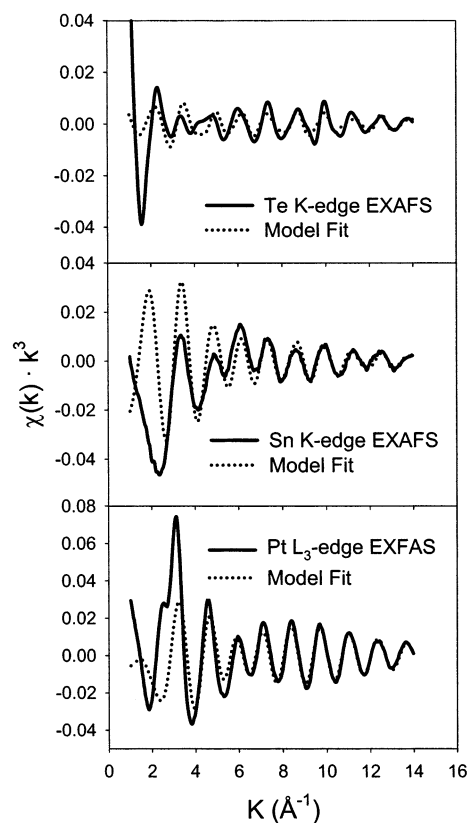

Figure 4. Illustration of the model used for EXAFS fitting. The model consists of a square planar platinum with four $Sn_2Te_6^{4-}$ clusters coordinating the central platinum through a single tellurium bridge. In this model, there is one unique tin site, one unique platinum site, and three unique tellurium sites.

Figure 5. Te, Sn, and Pt EXAFS data from hexagonal surfactant templated platinum tin telluride composites. The model fits are based on the cluster shown in Figure 4.

telluride cluster is integral to the formation of these platinum tin telluride materials. In agreement with this idea, recent experiments indicate that analogous composites can not be formed at room temperature using Pt^{2+}. Temperatures on the order of 80 °C appear to be needed to drive the reaction between Pt^{2+} and the $SnTe_4^{4-}$ cluster and cause precipitation of the composite. These results indicate that both solution phase reduction and solid-state redox chemistry may be important processes in the synthesis of these materials.

EXAFS Analysis. To learn about local bonding in these composites, analysis of the full EXAFS data is needed. Amorphous systems present a unique challenge for EXAFS analysis, however. Resolution of large lengthscale features is hindered due to the intrinsic disorder over these dimensions. Moreover, to account for multiple scattering, a model must be constructed to serve as the basis for fitting the data, and for disordered systems, a distribution of models is frequently more appropriate. In the platinum/tin/telluride composite system, however, all three nuclei of the inorganic framework can be analyzed using

EXAFS. The availability of information from three nuclei, which should be interdependent in this analysis, gives us a powerful tool to construct a model of our local structure.

Through a combination of initial fits using single scattering formalism and elemental analysis, a range of models were constructed (see Discussion). Of these, the model that best fits the data involves a four-coordinate, square planar platinum bonded to four Sn_2Te_6 clusters. The tin telluride dimer dimensions were taken from crystallographic data.[48] The model (Figure 3) was used to generate amplitude and phase shifts commensurate with single and multiple scattering paths. For the tellurium EXAFS model, there are three unique tellurium sites that need to be averaged together in the model to attain a meaningful fit. The averaging of unique sites is reflected in the noninteger N values seen in Table 1. Figures 5 and 6 show the
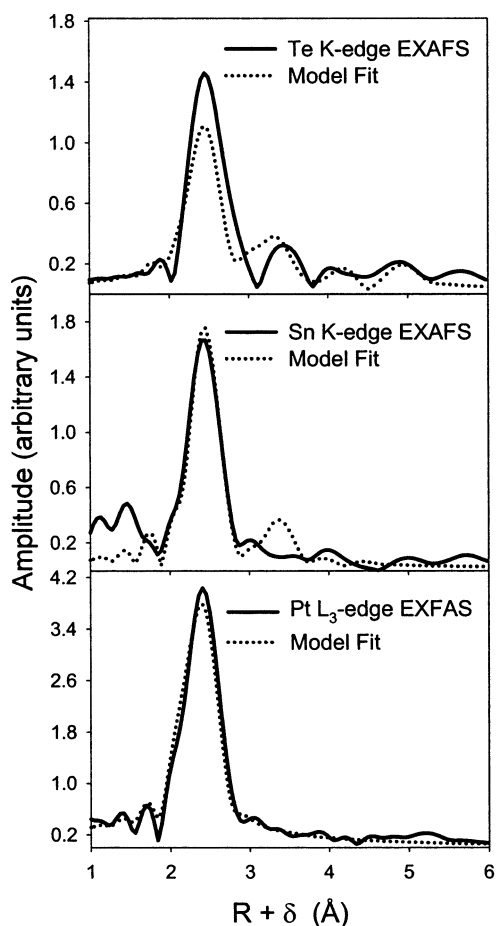
Figure 6. Fourier transformed Te, Sn, and Pt EXAFS with corresponding fits from the composite model shown in Figure 4. Good agreement is observed across nuclei, indicating that the model captures the sentient features of the local bonding in these nanoscale composite materials.

Table 2. Summary of Model Fit for Tin EXAFS

	N	R (Å)	$\sigma^2 (10^{-5} Å^2)$	ΔE_0
Te	1	2.65	260	−10.161
Te	1	2.76	270	−10.161
Te	2	2.78	272	−10.161
Pt	1	3.73	364	−10.161
Sn	1	4.42	432	−10.161

Table 3. Summary of Model Fit for Platinum EXAFS

	N	R (Å)	$\sigma^2 (10^{-5} Å)$	ΔE_0
Te	4	2.68	184	−4.903

EXAFS and Fourier transformed EXAFS of the platinum tin telluride composites along with model fits. Fit information is contained in Tables 1−3.

The platinum L_3 edge EXAFS is fit with a first shell model due to the lack of definition at larger R values. The first shell fits well to a square planar platinum coordinated by four tellurium at a distance of 2.68 Å. The tin EXAFS also fits the first shell well. Each tin is coordinated by four tellurium atoms, which have bond distances ranging from 2.65 to 2.78 Å. While there is some variance in these distances, they correlate well with the bond lengths of 2.68−2.80 Å found in single crystals of these clusters.[39] Past the first shell, the data remain relatively featureless, while the model predicts amplitude from a path that corresponds to a tin−platinum second shell coordination. The

amplitude of second shell coordinations are generally very sensitive to the local environment, and even small amounts of bond angle or bond length change can lower the amplitude significantly.[52] The first shell bond lengths compare well to expected values, which implies that variation in bond angles is leading to the lower amplitude at large R.

The tellurium EXAFS is the only nucleus that has multiple unique sites. As a result, the model that is used to fit the tellurium data is separated into three components: tellurium that bridges the platinum and tin, tellurium that bridges two tin, and single-coordinate dangling tellurium atoms. Each of these sites has the same population within the model, so they are weighed evenly. The fit to the spectra shows good first shell agreement. In the model, the first shell peak is a combination of the first shell tellurium−platinum and tellurium−tin distances. The tellurium−tin bond distance according to the tellurium EXAFS varies from 2.67 to 2.79 Å, which is in good agreement with the tin EXAFS distances. The tellurium−platinum coordination distance fits to 2.66 Å, which is also in excellent agreement with the platinum prediction of 2.68 Å.

The second shell tellurium coordinations show three main features. The first peak past the first shell coordination corresponds to a tellurium−tellurium interaction between diagonal tellurium in a square planar geometry on the platinum. The third peak also arises from the platinum square planar geometry; in this case it is a correlation between tellurium atoms that are diametrically opposite each other, bonded to the same platinum ion. The second low-intensity feature corresponds to tellurium−tellurium coordinations within a single tin telluride cluster. To appropriately fit this feature, a number of nearly identical paths must be removed to reduce intensity at this point so that the feature is fit by only one path. This indicates that there is disorder in the tin telluride tetrahedral structure. Because true disorder is almost impossible to include in a local model, we remove scattering paths to artificially account for this disorder. We note that the platinum square planar coordination remains consistent and well fit across nuclei. By contrast, disorder in the tin and tellurium EXAFS implies that the material, while retaining the $Sn_2Te_6^{x−}$ cluster, does experience significant distortion of the local tin environment.

C. Thermal and Optical Properties. The thermal stability of the platinum tin telluride was probed using thermogravimetric analysis. Figure 7 shows the mass loss as a function of temperature for a platinum tin telluride composite. The main feature of the TGA is the large (∼63%) mass loss starting around 150 °C. There is a sharp odor of tellurides after the analysis is done, indicating the loss of volatile tellurides. The percentage mass loss in the large step corresponds to loss of all organics and 75% of the tellurium in the composite. The composite does not retain structure after this treatment, which would be expected for a compositional change of this magnitude.

Band gap characterization was performed using near-IR/visible reflectance spectroscopy. Figure 8 shows the reflectance of a platinum tin telluride composite as a function of the energy of the incident beam. The spectrum shows a step at 0.8 eV, followed by a fairly constant, high-level absorption. The data indicate that this material is a narrow band gap semiconductor, with a band gap similar to bulk germanium (0.72 eV).

(52) Paesler, M. A.; Sayers, D. E.; Tsu, R.; Gonzales-Hernandez, J. *Phys. Rev. B* **1983**, *28*, 4550.
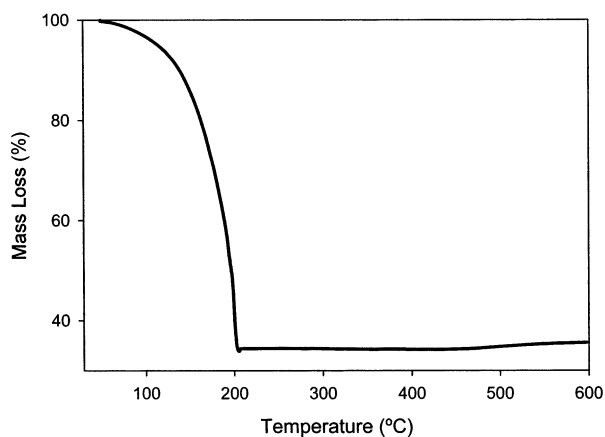
Figure 7. Thermogravimetric analysis of hexagonal platinum tin telluride composites. The large mass loss between 150 and 200 °C is associated with loss of all the organic from surfactant (including degradation of the surfactant and loss of residual solvent) combined with significant tellurium loss. The overall drop corresponds to loss of more than half of the tellurium in the composite.
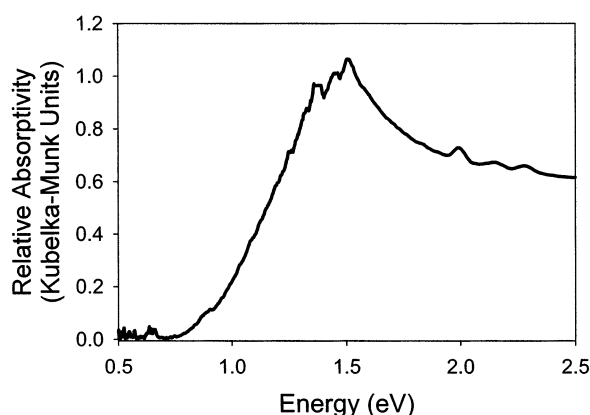

Figure 8. Near-IR/visible reflectance spectra of the hexagonal platinum tin telluride. A large absorption step occurs starting at 0.8 eV, indicating that this material is a narrow band gap semiconductor.

Discussion

The addition of platinum tetrachloride to a mixture of surfactant and tin telluride anions yields a material that is ordered on the nanometer size scale. While ion exchange has been used previously as a tool for promoting self-assembly in other non-oxide systems, those examples involve the use of intermediate valence transition metal ions (i.e., Fe^{2+}, Ni^{2+}, Pt^{2+}).[26−29] When divalent first-row elements are combined with surfactant and tin telluride anions, the result is almost always the formation of a layered phase.[53] By contrast, platinum(II) adducts, which tend to be more covalent, can form a hexagonal phase when coassembled with surfactant and tin telluride clusters, but elevated temperatures (∼80 °C) are needed to drive the assembly process.[53] This fact indicates that thermally activated ligand loss is needed prior to assembly with low valent platinum. As elevated temperatures frequently disfavor order in self-organized systems, we chose a higher valent ion so that less ligand loss (and thus lower temperatures) would be required to produce conditions favorable for electrostatic coassembly. Moreover, the platinum(IV) tin telluride system forms a robust solid product,

probably because of the redox chemistry that is available between the highly oxidized platinum and the reduced tin telluride cluster.

X-ray diffraction data confirm that assembly leads to a product with nanoscale periodicity. Both the thermal treatment and surfactant tail length, however, play important roles in determining the order of the final product. Longer surfactants lead to larger *d* spacings, which is consistent with simple surfactant packing arguments. While the cetyl and octadecyl surfactants show well-defined 2D hexagonal order, the longer eicosyl surfactant shows only a fundamental diffraction peak. The origin of this trend is probably thermal disordering of the surfactant molecules. In the water/silicate system, composites synthesized with C_{20}TEAB can undergo significant rearrangements, including phase transitions, due to thermal disorder of the long alkyl tails.[54] The heating, which is needed to optimize the atomic scale bonding, is probably increasing conformational disorder of the C_{20}TEAB tails, a fact that results in overall disorder in the structure.

EXAFS is used to conclude that the platinum in the composite is in a square planar geometry. Initial models included several platinum coordination geometries, including tetrahedral, octahedral, and square planar. Most models were discarded because of inconsistencies between fits for different nuclei. The models that yield the best correlation with the data contained platinum with a square planar geometry. The square planar geometry is consistent with d^8 platinum, which was predicted by the platinum(II) oxidation state as determined from the edge jump shift of the Pt EXAFS. Square planar platinum, however, can still be coordinated several different ways by the $Sn_2Te_6^{4−}$ clusters. The two most probable modes of coordination would be platinum with either two bidentate or four monodentate tin telluride dimers as ligands. Four monodentate dimers is in agreement with the elemental analysis and would be necessary to form a three-dimensional extended structure. Additionally, EXAFS models that involved bidentate cluster ligands were not consistent between nuclei.

The EXAFS model fits the data remarkably well for a disordered system. The first shell coordinations are well fit for all three nuclei, and the distances are consistent. This indicates that the local bonding around each nucleus is fairly regular. The square planar platinum geometry seems to be very regular, as there is little difference in bond length between each of the four tellurium−platinum bonds. Not only does the tellurium EXAFS confirm the regularity of the first shell bond lengths, but the fit also describes an undistorted square planar geometry with very regular bond angles. The strong amplitude of the second shell tellurium−tellurium coordinations (the diagonal and neighboring telluriums on the square of the square planar platinum) is a feature that is only expected to be seen for a highly regular $PtTe_4$ cluster.

The tin environment is slightly more disordered in comparison to the platinum coordination. In the first shell, there is a distribution of bond lengths, which indicates some variability in the tin tetrahedron. The second shell coordination to platinum predicted by the model does not show up in the tin data, further indicating significant bond angle disorder. This result is reasonable, given the literature on tin telluride clusters. While the simple $SnTe_4^{4−}$ species shows true tetrahedral bonding, higher

(53) Riley, A. E.; Tolbert, S. H. Unpublished results.

(54) Gross, A. F.; Ruiz, E. J.; Tolbert, S. H. *J. Phys. Chem. B* **2000**, *104*, 5448.

clusters such as $Sn_2Te_6^{4-}$ show a wide distribution of Te−Sn−Te bond angles, indicating that the system can accommodate significant deviation from ideal tetrahedral bonding.[39,49]

The tellurium EXAFS, when used in conjunction with the other nuclear EXAFS, confirms the regularity of the platinum sites and also shows that the tin is in a less regular geometry. The unique piece of information that the tellurium EXAFS provides is the average tellurium−tellurium distance within a tin telluride cluster, which is reasonable for the cluster geometries discussed above. The intensity of this peak, however, is much lower than would be expected from any of the models. The combination of ordered tellurium−platinum second shells and disordered tellurium−tin second shells in a single set of EXAFS data confirms the idea that the platinum ion coordination is very regular and the disorder in the system is localized to distortion of the tin telluride tetrahedra. Because the platinum tin telluride framework is forced to conform to a regular nanoscale architecture, some atomic level disorder needs to be present to accommodate the final structure. While the data do show some deviance from the model, our results suggest that the tin telluride clusters are more flexible at accommodating that disorder than the transition metal ions.

Thermogravimetric analysis indicates that this material is stable upon heating to 150 °C. The mass loss at this point is associated with surfactant decomposition, formamide, and tellurium loss. Volatile tellurides are a common oxidation product in air, and they are also expected to be liberated upon heating in nitrogen in the presence of organics. This loss of tellurium probably plays a key role in the loss of nanoscale periodicity that occurs upon heating to temperatures that promote organic decomposition. As a result, it does not appear that the thermal surfactant decomposition commonly employed to produce porous nanoperiodic oxide phases can be applied to these systems.

Solution phase ion-exchange methods have also been used to try to remove the organic from the composites. Treatment with a supported acid does lead to partial surfactant removal. However, the material does not exchange enough surfactant to produce porosity, as seen by gas adsorption/desorption measurements. Additionally, treatment with a supported acid leads to the formation of a less ordered phase with only one low-angle diffraction peak at a smaller repeat distance than the initial material.

One of the key reasons for moving away from oxide-based systems is to produce materials with broad absorption across the visible region and hopefully moderate conductivity. The band gap of these composites, as determined by near-IR/visible reflectance spectroscopy is 0.8 eV, consistent with a narrow band gap semiconductor. This is the smallest band gap reported to date for a nanostructured chalcogenide glass. Other chalcogenide-based mesostructured systems have been reported with band gaps ranging from 1.0 eV (NiGeSe) to 3.4 eV (ZnGeS).[47] As larger chalcogenides are used, the band gap decreases, probably due to better overlap of more diffuse orbitals. The PtSnTe value fits into this trend, increasing the range over which the band gap of nanostructured materials can be tailored.

Conclusion

A new inorganic/organic composite material with nanometer periodicity has been synthesized. By combining solid-state

synthesis of a reduced cluster anion with solution phase assembly techniques, a hexagonal mesophase was achieved. These materials are size tunable by changing the length of the surfactant tail. The local order was also probed using platinum, tin, and tellurium EXAFS. The amorphous nature of the system limits the modeling to a local system picture. However, on small length scales, there is significant information about the geometries of the different nuclei, which provides insight into the local structure of the inorganic framework.

Of particular interest is the platinum coordination. From work on the Ge_4S_{10} system, MacLachlan et al. predicted that a square planar geometry in the linking ion would be optimal for the formation of mesophases.[26] In mesophases, there is a need to balance the properties of a three-dimensional solid with the high surface area and quasi two-dimensional nature of the nanoscale inorganic wall. The square planar geometry can link inorganic clusters in a pseudo-two-dimensional manner, which could better match this structure. Both the edge position and the EXAFS fits predict that the $PtCl_4$ is reduced by the tin telluride clusters to d^8 Pt(II), which should adopt a square planar geometry. Additionally, the elemental data imply that the tin telluride clusters oligomerize in solution during the assembly process.

The importance of both oligomerization and oxidation during assembly and formation of the composite materials suggests that by controlling these factors, the final material and its structure can be controlled. For many applications, chemical control over the details of structural and electronic properties can potentially have important results. For example, in the case of thermoelectrics, where bulk tin telluride alloys have already been investigated, control over nanometer scale architecture may provide a means to optimize the interplay between thermal and electrical conductivity.[55,56]

The nanostructured platinum tin tellurides exhibit reflectivity characteristic of a narrow band gap semiconductor. Narrow band gap nanostructured materials show promise for a variety of applications that involve absorption of light. Specifically, the small band gap should allow facile production of photogenerated carriers. Although the voltage (and thus the external quantum efficiency) produced in such a photoexcitation event is small, the carrier production can be quite reasonable. As such, small band gap chalcogenide glasses have been found to be quite efficient for photocurrent applications.[57,58] Moreover, a variety of experiments on nanocrystal-based systems have shown that the high interfacial area of nanostructured materials can be used to efficiently separate electrons and holes in optoelectronic devices.[31−35] For nanocrystal-based systems, however, poor connectivity of the inorganic framework can make it hard to get these separate charge carriers to the collection electrodes. The morphology of the semiconducting frameworks presented here suggests that, in combination with appropriate electroactive organic templates, these materials could form the basis for highly efficient photocurrent devices.[59,60] These hexagonal platinum tin telluride nanocomposites display the unique combination of

(55) Vedeneev, V. P.; Krivoruchko, S. P.; Sabo, E. P. *Semiconductors* **1998**, *32*, 241.
(56) Heremans, J.; Thrush, C. M. *Phys. Rev. B* **1999**, *59*, 12579.
(57) Toyosawa, N.; Tanaka, K. *Phys. Rev. B* **1997**, *56*, 7416.
(58) Shimakawa, K. *Phys. Rev. B* **1986**, *34*, 8703.
(59) Lu, Y.; Yang, Y.; Sellinger, A.; Lu, M.; Huang, J.; Fan, H.; Haddad, R.; Lopez, G.; Burns, A. R.; Sasaki, D. Y.; Shelnutt, J.; Brinker, C. J. *Nature* **2001**, *410*, 913.
(60) Nguyen, T.-Q. Wu, J.; Doan, V.; Schwartz, B. J.; Tolbert, S. H. *Science* **2000**, *288*, 652.

high interfacial area, a homogeneous wall structure (which is needed to prevent trap sites), and broad absorption across visible and near-IR wavelengths.